Wilson, P.A., Lyle, M., and Firth, J.V. (Eds.)
Proceedings of the Ocean Drilling Program, Scientific Results Volume 199

22. Phosphorus and Barite Concentrations and Geochemistry in Site 1221 Paleocene/Eocene Boundary Sediments[1]

Kristina L. Faul[2], and Adina Paytan[3]

ABSTRACT

We determined changes in equatorial Pacific phosphorus (µmol P/g) and barite ($BaSO_4$; wt%) concentrations at high resolution (2 cm) across the Paleocene/Eocene (P/E) boundary in sediments from Ocean Drilling Program (ODP) Leg 199 Site 1221 (153.40 to 154.80 meters below seafloor [mbsf]). Oxide-associated, authigenic, and organic P sequentially extracted from bulk sediment were used to distinguish reactive P from detrital P. We separated barite from bulk sediment and compared its morphology with that of modern unaltered biogenic barite to check for diagenesis. On a $CaCO_3$-free basis, reactive P concentrations are relatively constant and high (323 µmol P/g or ~1 wt%). Barite concentrations range from 0.05 to 5.6 wt%, calculated on a $CaCO_3$-free basis, and show significant variability over this time interval. Shipboard measurements of P and Ba in bulk sediments are systematically lower (by ~25%) than shore-based concentrations and likely indicate problems with shipboard standard calibrations. The presence of Mn oxides and the size, crystal morphology, and sulfur isotopes of barite imply deposition in sulfate-rich pore fluids. Relatively constant reactive P, organic C, and biogenic silica concentrations calculated on a $CaCO_3$-free basis indicate generally little variation in organic C, reactive P, and biogenic opal burial across the P/E boundary, whereas variable barite concentrations indicate significant changes in export productivity. Low barite Ba/reactive P ratios before and immediately after the Benthic Extinction Event (BEE) may indicate efficient nutrient burial, and, if nutrient burial and

[1]Faul, K.L., and Paytan, A., 2005. Phosphorus and barite concentrations and geochemistry in Site 1221 Paleocene/Eocene boundary sediments. *In* Wilson, P.A., Lyle, M., and Firth, J.V. (Eds.), *Proc. ODP, Sci. Results,* 199, 1–23 [Online]. Available from World Wide Web: <http://www-odp.tamu.edu/publications/199_SR/VOLUME/CHAPTERS/214.PDF>. [Cited YYYY-MM-DD]
[2]Chemistry and Physics Department, Mills College, 5000 MacArthur Boulevard, Oakland CA 94613, USA. **kfaul@mills.edu**
[3]Department of Geological and Environmental Sciences, Stanford University, Stanford CA 94305, USA.

Initial receipt: 19 April 2004
Acceptance: 16 November 2004
Web publication: 8 July 2005
Ms 199SR-214

organic C burial are linked, high relative organic C burial that could temporarily drawdown CO_2 at this site. This interpretation requires postdepositional oxidation of organic C because organic C to reactive P ratios are low throughout the section. After the BEE, higher barite Ba/reactive P ratios combined with higher barite Ba concentrations may imply that higher export productivity was coupled with unchanged reactive P burial, indicating efficient nutrient and possibly also organic C recycling in the water column. If the nutrient recycling is decoupled from organic C, the high export production could be indicative of drawdown of CO_2. However, the observation that organic C burial is not high where barite burial is high may imply that either C sequestration was restricted to the deep ocean and thus occurred only on timescales of the deep ocean mixing or that postdepositional oxidation (burn down) of organic matter affected the sediments. The decoupling of barite and opal may result from low opal preservation or production that is not diatom based.

INTRODUCTION

The Paleocene–Eocene thermal maximum (PETM, ~55 Ma) was a time of abrupt global warming, when both deep-ocean and equatorial sea-surface temperatures increased significantly (Kennett and Stott, 1991; Thomas and Shackleton, 1996; Zachos et al., 1993, 2003). This event was accompanied by a foraminiferal benthic extinction event (BEE) (e.g., Miller et al., 1987; Thomas, 1998; Thomas and Shackleton, 1996) and a decrease in the carbon isotopic composition of marine carbonate of up to 3‰ (e.g., Bralower et al., 1995; Kennett and Stott, 1991; Thomas and Shackleton, 1996) during a period of ~30,000 yr and a gradual return to near-initial values during a period of ~150,000 yr (Norris and Röhl, 1999). These changes have been linked to massive release of biogenic methane from gas hydrate dissociation (e.g., Dickens et al., 1995, 1997) and imply that there were major perturbations in the global carbon cycle.

However, the nature of the response of marine export productivity to this event is controversial. Based on an increase in biogenic Ba (total Ba normalized for Ba crustal abundance) at Atlantic (Ocean Drilling Program [ODP] Site 1051) and Southern Ocean (ODP Site 690) sites, Bains et al. (2000) proposed that oceanic productivity increased during the PETM and may have been responsible for drawing down atmospheric CO_2, thereby cooling climate. Other evidence supporting increased marine productivity during the PETM includes a peak in biogenic Ba in the Middle Eastern bathyal sediments (Schmitz et al., 1997), Sr/Ca in coccolith carbonate at Site 690 (Stoll and Bains, 2003), and dinoflagellate assemblages that are indicative of increased productivity or increased temperature in coastal oceans (Crouch et al., 2001). Several other studies (e.g., Kelly et al., 1996; Bralower, 2002) have found evidence for decreased productivity for this interval at open-ocean sites in the equatorial Pacific (Site 865) and the Southern Ocean (Site 690) based on nannofossil assemblages. Dickens et al. (2003) proposed an alternative explanation for the increase in barite enrichment in PETM sediments—namely that this may have resulted from enhanced barite preservation because excess dissolved barium was released from seafloor gas hydrates. However, Ba/Ca data in foraminifers during this time interval are not consistent with this observation (Hall et al., 2004).

Understanding export production and organic C burial in the equatorial Pacific could have a major impact on interpretations of the causes and effects of this event. This area is an important upwelling zone and contributes to oceanic export productivity today as likely was also the case during the Paleocene and Eocene (Huber, 2002). We present here some of the first high-resolution records of reactive P and barite, indicators of nutrient burial and export production, respectively, across the Paleocene/Eocene (P/E) boundary in the equatorial Pacific Ocean.

We measured bulk sediment concentrations of reactive phosphorus (the sum of oxide-associated, authigenic, and organic P; sequentially extracted from bulk sediment), and barite ($BaSO_4$; wt%) at high resolution (2 cm) in P/E boundary sediments from ODP Leg 199 Hole 1221C (153.40–154.80 meters below seafloor [mbsf]). Reactive P was measured to separate the signal of P involved in biogeochemical cycling from detrital P. The measurement of barite (separated from bulk sediment) rather than biogenic Ba enabled us to identify the origin of the barite crystals (biogenic vs. diagenetic) by determining whether our samples resembled modern unaltered biogenic barite (Paytan et al., 2002).

Double peaks in total P and total Ba separated by a Mn peak and coincident with a low total Ca zone were measured in shipboard bulk sediment. Bulk Ca was measured on the ship to approximate calcium carbonate concentration in the P/E boundary sections from Sites 1220 and 1221 (Lyle, Wilson, Janecek, et al., 2002). These total concentration data were measured on bulk sediment samples using a lithium metaborate fusion procedure and are subject to shipboard analytical errors (e.g., error in weighing samples during high seas or instrumental noise levels varying with sea state; see discussion in Quintin et al., 2002). We compare our reactive P and total P values determined via sequential extraction in the laboratory to the shipboard total P values, which allows us to evaluate (1) the agreement between the measurements and (2) whether the biologically available P concentration (reactive P) is significantly different from total P. We compare barium concentrations associated with barite in each sample to the shipboard total Ba concentrations to determine the extent of detrital Ba influence on the total Ba concentrations.

We compare the reactive P and barite measurements to a suite of other biogenic productivity proxies ($CaCO_3$, organic C, and biogenic silica) generated by **Murphy et al.** (this volume). The multiproxy approach to paleoproductivity reconstructions is useful because strengths of some proxies compensate weaknesses of others (see Faul et al. [2003] for detailed evaluation of proxies and references). For example, sulfate reduction can lead to the loss of barite; otherwise, barite is a good export productivity tracer with a high burial efficiency (up to 30%) relative to other biogenic components (e.g., organic C and silica) (Dymond et al., 1992; Paytan et al., 1993; Paytan and Kastner, 1996).

Reactive forms of P delivered to the sediment/water interface, such as P associated with organic matter, are transformed to authigenic P with increasing age and depth in sediments (Ruttenberg and Berner, 1993; Delaney and Anderson, 1997, 2000; Filippelli and Delaney, 1995, 1996; Faul and Delaney, 2000; Faul et al., 2003). Because of this process, referred to as "sink-switching" by Ruttenberg and Berner (1993), the authigenic P phase provides an extractable record of nutrient (P) burial and thus a good indication of P cycling in the ocean. Since the vast majority of P flux to the sediment is associated with organic matter (Delaney, 1998), reactive P in the sediment may also represent organic C burial. The P burial record is preserved in sediments even when the

record of organic C is erased as a result of postdepositional oxidation (Anderson et al., 2001; Anderson and Delaney, in press). Here, we use reactive P as an indicator of nutrient P burial and also as a proxy related to organic C burial. We use the ratio of barite to reactive P in sediments as a measure of the ratio of organic matter exported from the surface ocean to depth to nutrients and organic C buried in the sediment. This comparison holds as long as barium and phosphorus are not remobilized diagenetically (Nilsen et al., 2003). We assess what these records may indicate about equatorial Pacific productivity and the potential role of export production on C sequestration across the P/E boundary.

METHODS

We used 5-cm³ samples for phosphorus determinations and 10-cm³ samples for barite extractions at continuous 2-cm intervals from 153.40 to 154.8 mbsf, which corresponds to the PETM (Section 199-1221C-11H-3) recovered at Leg 199 Site 1221. The 10-cm³ samples were washed through a 63-µm sieve, and both size fractions were retained. The >63-µm fraction was oven-dried and analyzed (by other researchers) for foraminiferal isotopes. We used the <63-µm fraction for barite separations. Individual fine fraction sample weights ranged from 5 to 10 g. Because sample weights were much smaller than those typically used for barite separations (e.g., 20–30 g) (Paytan et al., 1996; Eagle et al., 2003), a subset of initial samples were combined to represent 4-cm intervals (50–54, 54–58, 58–62, 62–66, and 66–70 cm) to ensure that enough barite would be extracted for analysis. However, barite yields were so high that combining samples was deemed unnecessary and was not done for the remainder of the samples.

We separated barite from sediment samples using a sequential leaching procedure that included reaction with hydrochloric acid (6 N), warm (50°C) sodium hypochlorite (5 wt%), warm (80°C) hydroxylamine (0.02 N) in acetic acid (0.05 M), and 1:2, 1:1, and 2:1 hydrofluoric acid (40 wt%):nitric acid (1 N) mixtures (Paytan et al., 1993; Eagle et al., 2003). This procedure dissolves carbonates, oxidizes organic matter, removes transition metal oxyhydroxides, dissolves siliceous material, and removes fluorides in order to isolate barite. After weighing the sample separation residues, we used a back-scattered electron imaging detector mounted on a scanning electron microscope (SEM) and the EDAX Image/Mapping program to determine the percent barite in the residues and to examine barite crystal morphology. Most sample residues in this study were found to be ~100% barite upon examination. This procedure is detailed in Eagle et al. (2003).

We used a four-step, operationally defined sequential P extraction (Anderson and Delaney, 2000) modified from a five-step P extraction procedure (SEDEX) (Ruttenberg, 1992) to determine P concentrations in four sedimentary components: oxide-associated P (includes P sorbed to and incorporated in oxyhydroxides), authigenic P (authigenic carbonate fluoroapatite), organic P (acid insoluble P), and detrital P (terrestrial silicates and detrital apatite). An additional first step of water-soluble P was extracted for randomly chosen samples (Table T1) to determine whether there is a contribution of water-soluble P to total P in deep-sea sedimentary samples. Water-soluble P is a significant source of P in sediment trap samples (Faul et al., in press). However, since most water-soluble P is typically remobilized before reaching the sediments, this

T1. P and $BaSO_4$ concentrations, p. 20.

fraction is insignificant for deep-sea sedimentary samples and will not be discussed further.

We determined P concentrations on splits of the 5-cm³ bulk samples. After freeze-drying the samples, we crushed the samples and passed them through a 150-µm sieve to ensure uniformity in particle size. After extracting the four components of P into known volumes of extractant from replicate samples (~0.1 g), we used a Lachat Quick Chem 8000 automated spectrophotometric flow injection analysis system to measure P concentrations. Results are reported as the means ±1σ (sample standard deviation) of duplicate runs. Reactive P is calculated as the sum of water-soluble P (when appropriate), oxide-associated P, authigenic P, and organic P, with errors propagated from errors on individual components. Total P is the sum of reactive P and detrital P.

The long-term analytical reproducibility was assessed by calculation of the mean P concentrations ±1σ for two sedimentary consistency standards (Table T2). One of the two was processed and measured with each run as a sample. Consistency standard relative errors are similar to those from other sedimentary P studies (e.g., Filippelli and Delaney, 1995, 1996; Anderson and Delaney, 2000). The relative errors of the long-term means of the consistency standards were high for components that were close to detection limit and constituted small fractions of total P for the standards. Relative fractions in these consistency standards are very similar to those of the samples analyzed here. Typical sample concentrations well exceeded the detection limits by a minimum factor of 10 for oxide-associated P and up to a factor of 350 for authigenic P (Table T2).

$CaCO_3$-free concentrations of reactive P, detrital P, barite, and shipboard Mn were calculated using $CaCO_3$ values generated by **Murphy et al.** (this volume). Organic C to reactive P values were calculated using $CaCO_3$-free organic C (**Murphy et al.,** this volume) and $CaCO_3$-free reactive P.

RESULTS

We compared total P as calculated from the sum of all of the P extraction steps to shipboard total P values (Fig. F1A; Tables T1, T3). The shipboard P concentrations are lower than the sequential extraction P concentrations by ~25% (slope = 0.74 ± 0.06) (Fig. F1B), especially where total P is high (e.g., at ~154.00 mbsf and in the interval 154.2–154.3 mbsf) (Fig. F1A). At low to moderate values, the shipboard total Ba measurements are higher than the barite Ba concentrations (Fig. F2A). However, for samples with high barite concentrations at ~154.1 mbsf and between 154.2 and 154.3 mbsf, the shipboard-measured total Ba values are lower than the barite Ba concentrations (Fig. F2A). Shipboard Ba values are systematically offset from barite Ba concentrations by ~25% (slope = 0.75) (Fig. F2B).

Consistent with many studies of deep-sea sedimentary P (Delaney and Anderson, 1997, 2000; Filippelli and Delaney, 1995, 1996; Faul and Delaney, 2000; Faul et al., 2003), most reactive P in these sediments (96% ± 14%) is in the form of authigenic P (Table T1). The concentrations of P in the other reactive sedimentary components (water soluble, oxide-associated, and organic P) are extremely low and compose <2% of total P (Table T1). Authigenic P determined according to the operationally defined sequential extraction procedure (Ruttenberg 1992) may include fish teeth (biogenic carbonate fluorapatite). Indeed, several fish

T2. Analytical figures, p. 21.

F1. Total P and shipboard P, p. 16.

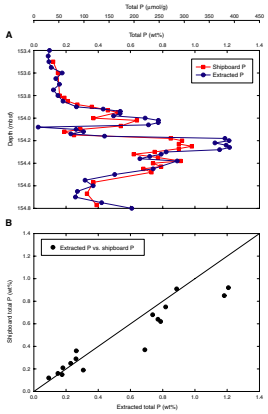

T3. Shipboard P, $BaSO_4$, and Mn, p. 22.

F2. Barite and shipboard Ba, p. 17.

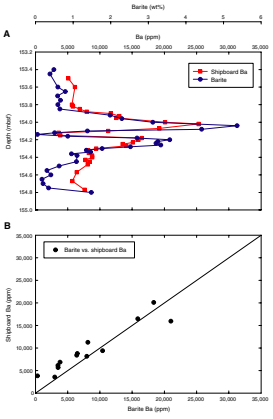

teeth were found in samples from Section 199-1221C-11X-3 (samples from 24 to 44 cm [~153.65–153.85 mbsf], R. Norris, pers. comm., 2004). However, both Froelich et al. (1982) and Anderson et al. (2001) have demonstrated that fish debris constitutes an insignificant percentage of both the global P budget and typical oceanic authigenic P concentrations. A typical fish tooth contributes ~0.12 µmol P/g sediment to authigenic P (Faul et al., 2003). Authigenic P concentrations for this site are typically two to three orders of magnitude higher (Table T1). Given these P concentrations, fish teeth are an insignificant portion of authigenic P concentrations in this study.

We separate reactive P from detrital P (Fig. F3) because detrital P is not involved in biological cycling of P. In these sediments, it is particularly important because detrital P concentrations are high (as high as 76 µmol P/g or 0.24 wt%) and compose a significant portion of total P from 154.5 to 154.18 mbsf (19% of total P) but drop to almost zero (1.4 µmol P/g or 0.004 wt%) at 154.16 mbsf (e.g., 1% of total P) (Table T1, Fig. F3). Because this detrital P is included in total P but is not biologically reactive, total P would overestimate reactive P in some intervals. Moreover, a change in biologically related P burial but not in detrital P (154.04 mbsf) could be masked when looking only at total P. Reactive P concentrations peak at 300 µmol P/g immediately after the BEE (Lyle, Wilson, Janecek, et al., 2002) then decrease to as low as 7.5 µmol P/g, coincident with the shipboard-measured Mn peak, and then increase 20 cm upcore, showing a secondary peak of ~250 µmol P/g at 154.04 mbsf (Table T1; Fig. F3).

Barite concentrations in the sediments range from 0.05 wt% to as high as 5.4 wt%, peaking simultaneously with reactive P burial (Table T1; Fig. F3). Like P, barite concentrations exhibit a double peak; however, in the case of barite, the relative size of the peaks is reversed (Table T1; Fig. F3). Peak values of barite concentrations (~5.4 wt% or ~31,000 ppm) are higher than any others observed for P/E boundary sediments to date. For example, maximum biogenic Ba concentrations for the North Atlantic (Hole 1051B) are ~2000 ppm and are ~1000 ppm (Bains et al., 2000) for the Southern Ocean (Hole 690B). Examination of all separated barite samples from this core by SEM indicates that our samples resemble modern unaltered biogenic barite and thus are not of diagenetic origin. The barite crystals are the size (2–5 µm) and morphology (euhedral) of modern unaltered biogenic barite and are considerably better preserved than barite from other P/E boundary cores (e.g., Hole 1051B) (Bains et al., 2000).

$CaCO_3$ values as measured by **Murphy et al.** (this volume) decrease from 74 to 1 wt% in the interval from 154.70 to 153.26 mbsf, remain at <5 wt% until 154.02 mbsf, and then recover to ~80 wt% at 153.85 mbsf (Table T4; Fig. F1). To remove the effect of changes in $CaCO_3$ content on the calculated barite and P concentrations, we determined these concentrations also on a $CaCO_3$-free basis. When calculated on a $CaCO_3$-free basis, most of the variation in reactive P is removed (Table T4, Fig. F4A). $CaCO_3$-free reactive P concentrations hover around 1 wt% (323 µmol P/g) except in the interval from 154.2 to 154.0 mbsf, where $CaCO_3$-free reactive P values drop to as low as 0.02 wt% (Table T4, Fig. F4A). Changes in $CaCO_3$ significantly affect the shape of the record of reactive P, suggesting that P concentration changes are mainly a function of the dilution rate by carbonate, although they do not completely drive the record (Figs. F3, F4). For example, the reactive P concentrations increase (154.06 mbsf) before the $CaCO_3$ concentrations

F3. Geochemical components vs. depth, p. 18.

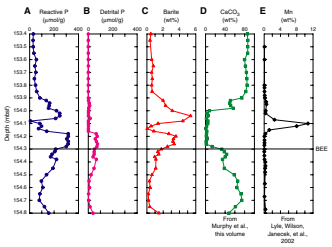

T4. $CaCO_3$, $CaCO_3$-free concentrations, and reactive P ratios, p. 23.

F4. $CaCO_3$-free concentrations and barite Ba to reactive P ratio, p. 19.

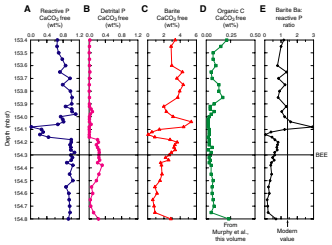

increase (154.0 mbsf). Detrital P, barite, and shipboard Mn concentrations yield similar distribution trends (although they change in magnitude) whether calculated on a $CaCO_3$-free basis or not (Figs. F3, F4; Tables T1, T4).

Organic C to reactive P ratios yield values (0.26 ± 0.34) (Table T4) consistently lower than the Redfield Ratio (117:1) (Anderson and Sarmiento, 1994), indicating preferential loss of C in the water column during deposition or in the sediment at some point after burial. A calculated barite/reactive P ratio for a modern equatorial Pacific core top (JGOFS TT013-69MC, 0.11°N, 139.72°W; 4307 meters below sea level) is 1.4 (molar ratio), based on measured values of Ba associated with barite (Eagle et al., 2003) and reactive P (Faul et al., in press) in this core top. In comparison, the barite/reactive P ratio for the PETM range at ODP Site 1221 ranges from much lower than modern value (as low as 0.05 at 154.14 mbsf) to higher than modern value (2.9 at 154.08 mbsf) (Table T4; Fig. F4). These changing ratios may indicate changes in export productivity relative to nutrient burial during the PETM interval.

Shipboard results show an Mn peak (~12 wt%) (Lyle, Wilson, Janecek, et al., 2002) when $CaCO_3$ values are low (Fig. F3; Tables T3, T4). Visual inspection revealed the presence of small manganese oxide nodules in several samples from the section (R. Norris, pers. comm., 2004).

DISCUSSION

Shipboard to Shore-Based Data Comparison

Poor reproducibility or discrepancies in phases dissolved by different procedures are unlikely to account for the systematic offset observed in shipboard to shore-based P and barite values. Neither the sequential extraction reproducibility (~4%) nor the shipboard reproducibility (10%–15%) (Quintin et al., 2002) can account for a systematic difference. It is unlikely that the difference could be accounted for in terms of detrital P (or some other phase) not being extracted in the shipboard procedure, causing the shipboard total P values to be systematically lower than shore-based total P values. Detrital P values from the sequential extraction are high in the interval from 154.1 to 154.5 mbsf (Figs. F3, F4), but the largest difference between the sequential extraction total P and the shipboard total P exists in the interval between 154.2 and 154.3 mbsf (Fig. F1). In contrast, some of the offset between shipboard Ba and shore-based barite could be explained by the fact that the shipboard procedure includes detrital Ba in addition to barite. Additionally, the fluxing may not have quantitatively dissolved all of the barite where the barite content was substantial. Indeed, the cross-plot between the shipboard total Ba and the barite extraction–based Ba indicates a residual amount of detrital Ba of ~3000 ppm, (Fig. F2B). However, the fact that the slope between shipboard and shore-based values is 25% lower than 1:1 cannot be accounted for by the addition of detrital Ba. We believe that the discrepancy between shipboard and shore-based measurements can only be accounted for by problems with calibration of the shipboard standards for high P and Ba concentrations. Indeed, Quintin et al. (2002) point out that it was a challenge to find standard reference materials to cover the range of elemental concentrations encountered during Leg 199.

Effects of Changing $CaCO_3$

As a preliminary substitute for mass accumulation rates and to account for dilution effects, we determine concentrations on a $CaCO_3$-free basis. The interval of low $CaCO_3$ concentrations (<5 wt%; 154.3–154.0 mbsf) (Fig. F3) indicates either dissolution (most likely) or nondeposition of $CaCO_3$, the predominant biogenic sedimentary component. The sharp and simultaneous drop-offs of reactive P, detrital P, and barite at ~154.2 mbsf (Figs. F3, F4) may indicate that an interval of extremely low deposition of all components may be present in this section, although it is impossible to determine definitively if indeed the deposition rates in this interval were low without a determination of precise sedimentation rates (on the timescale of the observed sedimentary changes). If, however, the sedimentation rates throughout the section were constant, the accumulation rate records would show the same trends in reactive P and barite abundances as those presented here. In any case, interpretations made on a $CaCO_3$-free basis should be a good first-order substitute for mass accumulation rate trends. Moreover, the relative magnitudes of the different proxies at the same depth horizons will remain the same regardless of absolute values. That is, the organic C to reactive P ratios as well as the barite to reactive P ratios and any other comparisons of the different proxies at the same depth horizons will be unaffected by sedimentation rate or dilution effects by carbonate. Thus, we believe the lack of accumulation rate data does not preclude preliminary paleoceanographic interpretation of our results.

Evidence for Oxygenation of the Sediments

The presence of Mn oxide nodules, the high barite concentrations, and the similarity of the barite to modern unaltered barite, along with low organic C in the sediments, imply that there were oxygenated conditions in the sediments during the PETM at this site in the eastern equatorial Pacific and that at some point, either during the PETM or postdepositionally, organic C was lost from the section. The presence of solid MnO_2 (nodules) forming at the sediment/water interface indicates oxygenated bottom water conditions (Calvert and Pedersen, 1993). The Mn peak may be attributed to diagenetic mobilization of Mn in reducing conditions followed by precipitation upon oxidation. This, however, is not consistent with the occurrence of the nodules. Sulfate concentrations in the pore waters at present throughout the core are similar to seawater value (28 mM) (Lyle, Wilson, Janecek, et al., 2002). Both the morphology and the sulfur isotopes in the barite indicate that the barite is not diagenetically formed in reducing pore fluids. Thus, there is no indication that sulfate was deficient enough in these sediments to dissolve barite at the time of the PETM or at any time since, supporting the use of barite at this site as an export production proxy.

Evidence for Constant Organic C Burial

Because sink-switching retains the reactive P initially delivered to the sediment predominantly with organic C, reactive P may be used as an indicator of P burial and for initial organic C deposition even at sites where postdepositional oxidation removed the organic matter (Anderson et al., 2001; Anderson and Delaney, in press, Faul et al., in press). Reactive P concentrations are high (~1 wt%) and relatively constant on

a $CaCO_3$-free basis (except from 154.2 to 154.0 mbsf) (Fig. F4). In contrast, the organic C values are very low (average = 0.06 wt% calculated on a $CaCO_3$-free basis). Organic C to reactive P ratios (0.02–2.2) (Table T4) are much lower than the Redfield Ratio (117) and thus indicate preferential loss of organic C relative to reactive P at this site. These combined observations along with high barite burial suggest that much of the organic C may have been oxidized and/or captured in forms that are difficult to measure. The biogenic silica records also show no changes in biogenic opal deposition across the boundary when calculated on a $CaCO_3$-free basis (**Murphy et al.,** this volume), and if diatoms are responsible for a large fraction of organic matter flux or if their abundance is proportional to organic matter flux, this also indicates that no significant change in organic C delivery to the sediments across the PETM has occurred, assuming no changes in preservation over the sampled time. Reactive P trends are inversely correlated with $CaCO_3$ content throughout much of the interval. Presumably, as indicated by our carbonate-free calculations, reactive P deposition remained constant (except for the interval from 154.2 to 154.0 mbsf) and the $CaCO_3$ diluted or enhanced the reactive P signal. This scenario is consistent with little change in P and presumably organic C burial across the section.

Evidence for Changes in Export Production and Nutrient Cycling Efficiency

In the modern ocean, productivity tracers in the sediment do not always co-vary, even under areas of high production. In oxygenated sediments under the high export productivity region of the equatorial Pacific, organic C contents of the sediments are low whereas barite contents are high (Paytan et al., 1996). This is the case for these PETM sediments. High barite concentrations may be interpreted as indicating high export productivity at this site. This high export production scenario may be consistent with low organic C burial if organic C is lost postdepositionally and/or if organic C is efficiently regenerated in the deep ocean before burial. The barite/reactive P ratio can act as a measure of the efficiency of internal nutrient cycling (Nilsen et al., 2003). A high barite Ba/reactive P ratio may indicate a time of higher export production associated with a low net nutrient burial, whereas a low barite Ba/reactive P ratio may indicate a time of lower export production and high net nutrient burial. The records of barite and reactive phosphorus during the PETM show variation in barite/reactive P ratios both above and below the modern measured core top equatorial Pacific value of 1.4 (Table T4; Fig. F4). Lower than modern barite Ba to reactive P ratios before the BEE and immediately afterward indicate efficient nutrient burial compared to export production relative to today's equatorial Pacific sites. In contrast, a high barite Ba to reactive P ratio (2.9) at 154.08 mbsf and subsequent values similar to those today (but higher than the pre-BEE values) may indicate higher export production, as evidenced by elevated barite, coupled with more efficient nutrient recycling, as evidenced by unchanging nutrient (P) burial. Efficient nutrient regeneration (e.g., reactive P regeneration preferentially to organic C) could drive and sustain high primary productivity while increasing net organic C burial, but the low organic C to reactive P ratios found in this core do not support preferential reactive P regeneration, unless C was lost postdepositionally.

Reconciliation of Differing Productivity Signals

Changes in export production and nutrient-recycling efficiency that are decoupled from each other could reconcile differing signals observed in reactive P, organic C, and barite for this site in the eastern equatorial Pacific. Constant and relatively low organic C and biogenic opal sedimentation, along with relatively constant reactive P, indicate little change in the organic C burial and possibly organic C delivery to the site. However, both export productivity, as evidenced by high barite concentrations, and nutrient burial efficiency, as evidenced by high reactive P concentrations, were higher before the BEE than today. If reactive P and organic C burial are linked, this could signify a situation where organic C could have been sequestered in the sediments, therefore drawing down CO_2. The low organic C to reactive P ratios in the sediment at present most likely result from postdepositional loss of organic C.

After the interval of presumably low sedimentation (beginning at ~154.18 mbsf), both nutrient burial (P) and export productivity (barite) increase but export productivity increases more than nutrient burial, as evidenced by higher average barite Ba/reactive P ratios, indicating that nutrient recycling efficiency has increased approximately to the level it is at today. Two specific scenarios may be envisioned for this time interval. The first requires high export of organic matter below the euphotic zone, which results in barite formation and burial while the reactive P is recycled within the euphotic zone efficiently to sustain productivity. This would require decoupling of organic C from reactive P in the water column. Alternatively, reactive P is recycled in the deep ocean and/or at the sediment/water interface along with organic C, resulting in lower burial of reactive P and organic C. The latter option will result in C sequestration only on timescales of ocean water turnover (thousands of years) and not on longer timescales. The former option results in more effective long-term C sequestration. Thus, high export flux (as indicated by a peak in barite burial) and efficient P recycling in the euphotic zone (as indicated by constant reactive P burial), presumably decoupled from C recycling, would result in C being delivered and buried in the sediment (as suggested by the barite peak). Organic C would then be lost to oxidation at some time after deposition (consistent with the very low C to P ratios and Mn peak).

As indicated above, changes in the relative rates of export production, nutrient and organic C recycling efficiency, and organic C and nutrient burial along with postdepositional loss of organic C may explain the observed fluctuations in the sedimentary record at this site across the P/E boundary. Because our data are limited to one location, we cannot globally extrapolate our conclusions for the nature of either export productivity or nutrient burial. However, efficient nutrient and organic C recycling may explain widespread indications of increases of productivity in the surface waters and high export production (e.g., Sr/Ca ratios in coccolith carbonate at Site 690 [Stoll and Bains, 2003]). When postdepositional oxidation of organic C is invoked, this is also consistent with low organic C burial for the PETM. If, indeed, C was originally buried in the sediment and was subsequently lost, as may be suggested by the high (albeit constant) reactive P, the Mn peak, and the high barite, then longer-term C sequestration may have taken place. However, until further direct constraints regarding the timing of C regeneration are available it is not possible to distinguish between the two scenarios postulated above. Regardless, these mechanisms provide an explana-

tion for high barite concentrations despite low organic C deposition without necessarily invoking Ba release from methane clathrates (Dickens et al., 2003).

CONCLUSIONS

We determined changes in equatorial Pacific P burial and barite concentrations across the P/E boundary in sediments from ODP Leg 199 Site 1221 (153.40–154.80 mbsf at 2 cm resolution). Reactive phosphorus (the sum of oxide-associated, authigenic, and organic P; sequentially extracted from bulk sediment) was used to distinguish the signal of P involved in biogeochemical cycling from detrital P, a measure that can be used for determining organic C delivery and burial in the sediment even when organic C is oxidized postdepositionally. On a $CaCO_3$-free basis, reactive P concentrations are high but relatively constant at ~1 wt% and show little change across the section, with the exception of lower values from 154.2 to 154.0 mbsf. Barite concentrations for the sediments range from 0.05 to 5.6 wt% calculated on a $CaCO_3$-free basis. Barite shows a distinct peak at 154.08 mbsf. Barite Ba/reactive P ratios in the sediments are low (average = 0.48 from 154.8 to 154.20 mbsf) before and immediately after the BEE and similar to or higher than modern values (average = 1.1 from 154.04 to 153.40 mbsf) after the BEE (Table **T4;** Fig. **F4**), even though both barite and reactive P concentrations are higher than modern core top values. Observed organic C to reactive P ratios (0.26 ± 0.34) (Table **T4**) are lower than the Redfield Ratio (117:1) (Anderson and Sarmiento, 1994) potentially suggesting organic C loss after burial.

Despite the lack of sedimentation rates, the use of $CaCO_3$-free based calculations and elemental ratios (although not ideal) allow us to make preliminary conclusions about oxygenation, nutrient cycling and burial, and export productivity at this site across the PETM. The presence of Mn oxide nodules and the size, morphology, and sulfur isotopes of barite imply that these sediments were oxygenated or at least not sulfate reducing during the PETM. Relatively constant reactive P, organic C, and biogenic silica concentrations indicate little variation in organic C burial across the interval, whereas a peak in barite concentration indicates fluctuations in export productivity. Fluctuations in the barite/reactive P ratios along the interval may indicate changes in the efficiency of organic C export from the photic zone vs. nutrient and organic C burial in the sediments. Organic C must have been oxidized sometime after deposition to explain the low C to P and barite ratios. After the BEE, higher barite/reactive P ratios may indicate higher export productivity coupled with more efficient organic C and reactive P regeneration in the water column. Efficient organic matter recycling, despite high export productivity, indicates only short-term (timescale of deepwater mixing) drawdown of CO_2 occurred as indicated by the low organic C burial in the sediments. Differences in export productivity and organic C burial and postdepositional alteration of sedimentary records may help explain discrepancies in productivity proxies from the same sites during the PETM and may be indicative of various water column and postdepositional biogeochemical processes.

ACKNOWLEDGMENTS

We are grateful to Professor Margaret Delaney, University of California Santa Cruz (UCSC), for the use of her laboratory to prepare and analyze bulk sediment for phosphorus concentrations. We thank R. Franks and the UCSC Institute of Marine Sciences Marine Analytical Laboratory. This research used samples and/or data provided by the Ocean Drilling Program (ODP). ODP is sponsored by the U.S. National Science Foundation (NSF) and participating countries under management of Joint Oceanographic Institutions (JOI), Inc. The U.S. Science Support Program (USSSP funding to KLF and AP) and NSF Grant 0120727 (subaward to M.L. Delaney; J.C. Zachos, principal investigator) provided funding for this research. We thank the ODP Leg 199 Scientific Party.

REFERENCES

Anderson, L.A., and Sarmiento, J.L., 1994. Redfield ratios of remineralization determined by nutrient data analysis. *Global Biogeochem. Cycles,* 8:65–80.

Anderson, L.D., and Delaney, M.L., 2000. Sequential extraction and analysis of phosphorus in marine sediments: streamlining of the SEDEX procedure. *Limnol. Oceanogr.,* 45:509–515.

Anderson, L.D., and Delaney, M.L., in press. Middle Eocene to early Oligocene paleoceanography from Agulhas Ridge, Southern Ocean (ODP Leg 177, Site 1090). *Paleoceanography.*

Anderson, L.D., Delaney, M.L., and Faul, K.L., 2001. Carbon to phosphorus ratios in sediments: implications for nutrient cycling. *Global Biogeochem. Cycles,* 15:65–79.

Bains, S., Norris, R.D., Corfield, R.M., and Faul, K.L., 2000. Termination of global warmth at the Palaeocene–Eocene boundary through productivity feedback. *Nature (London U.K.),* 407:171–174.

Bralower, T.J., 2002. Evidence of surface water oligotrophy during the Paleocene–Eocene Thermal Maximum: nannofossil assemblage data from Ocean Drilling Program Site 690, Maud Rise, Weddell Sea. *Paleoceanography,* 17(2):10.1029/2001PA000662.

Bralower, T.J., Zachos, J.C., Thomas, E. Parrow, M., Paull, C.K., Kelly, D.C., Premoli Silva, I., Sliter, W.V., and Lohmann, K.C., 1995. Late Paleocene to Eocene paleoceanography of the equatorial Pacific Ocean: stable isotopes recorded at Ocean Drilling Program Site 865, Allison Guyot. *Paleoceanography,* 10:841–865.

Calvert, S.E., and Pedersen, T.F., 1993. Geochemistry of Recent oxic and anoxic marine sediments: implications for the geological record. *Mar. Geol.,* 113:67–88.

Crouch, E.M., Heilmann-Clausen, C., Brinkhuis, H., Morgans, H.E.G., Rogers, K.M., Egger, H., and Schmitz, B., 2001. Global dinoflagellate event associated with the Late Paleocene Thermal Maximum. *Geology,* 29:315–318.

Delaney, M.L., 1998. Phosphorus accumulation in marine sediments and the oceanic phosphorus cycle. *Global Biogeochem. Cycles,* 12:563–572.

Delaney, M.L., and Anderson, L.D., 1997. Phosphorus geochemistry in Ceara Rise sediments. *In* Shackleton, N.J., Curry, W.B., Richter, C., and Bralower, T.J. (Eds.), *Proc. ODP, Sci. Results,* 154: College Station, TX (Ocean Drilling Program), 475–482.

Delaney, M.L., and Anderson, L.D., 2000. *Data report:* Phosphorus concentrations and geochemistry in California margin sediments. *In* Lyle, M., Koizumi, I., Richter, C., and Moore, T.C. (Eds.), *Proc. ODP, Sci. Results,* 167: College Station, TX (Ocean Drilling Program), 195–202.

Dickens, G.R., Castillo, M.M., and Walker, J.G.C., 1997. A blast of gas in the latest Paleocene: simulating first-order effects of massive dissociation of oceanic methane hydrate. *Geology,* 25:259–262.

Dickens, G.R., Fewless, T., Thomas, E., and Bralower, T.J., 2003. Excess barite accumulation during the Paleocene–Eocene Thermal Maximum: massive input of dissolved barium from seafloor gas hydrate reservoirs. *In* Wing, S.L., Gingerich, P.D., Schmitz, B., and Thomas, E. (Eds.), *Causes and Consequences of Globally Warm Climates in the Early Paleogene*. Spec. Pap.—Geol. Soc. Am., 369:11–23.

Dickens, G.R., O'Neil, J.R., Rea, D.K., and Owen, R.M., 1995. Dissociation of oceanic methane hydrate as a cause of the carbon isotope excursion at the end of the Paleocene. *Paleoceanography,* 10:965–971.

Dymond, J., Suess, E., and Lyle, M., 1992. Barium in deep-sea sediment: a geochemical proxy for paleoproductivity. *Paleoceanography,* 7:163–181.

Eagle, M., Paytan, A., Arrigo, K.R., van Dijken, G., and Murray, R.W., 2003. A comparison between excess barium and barite as indicators of carbon export. *Paleoceanography,* 18(1):10.1029/2002PA000793.

Faul, K.L., Anderson, L.D., and Delaney, M.L., 2003. Late Cretaceous and early Paleogene nutrient and paleoproductivity records from Blake Nose, western North Atlantic Ocean. *Paleoceanography,* 18(2):10.1029/2001PA000722.

Faul, K.L., and Delaney, M.L., 2000. Data report: Phosphorus concentrations and geochemistry in Blake Nose sediments from Leg 171B. *In* Kroon, D., Norris, R.D., and Klaus, A. (Eds.), *Proc. ODP, Sci. Results,* 171B, 1–10 [CD-ROM]. Available from: Ocean Drilling Program, Texas A&M University, College Station TX 77845-9547, USA.

Faul, K.L., Paytan, A., and Delaney, M.L., in press. Phosphorus distribution in oceanic particulate matter. *Mar. Chem.*

Filippelli, G.M., and Delaney, M.L., 1995. Phosphorus geochemistry and accumulation rates in the eastern equatorial Pacific Ocean: results from Leg 138. *In* Pisias, N.G., Mayer, L.A., Janecek, T.R., Palmer-Julson, A., and van Andel, T.H. (Eds.), *Proc. ODP, Sci. Results,* 138: College Station, TX (Ocean Drilling Program), 757–767.

Filippelli, G.M., and Delaney, M.L., 1996. Phosphorus geochemistry of equatorial Pacific sediments. *Geochim. Cosmochim. Acta,* 60:1479–1495.

Froelich, P.N., Bender, M.L., Luedtke, N.A., Heath, G.R., and DeVries, T., 1982. The marine phosphorus cycle. *Am. J. Sci.,* 282:474–511.

Hall, J.M., Zachos, J.C., Turekian, K.K., 2004. Increased barite precipitation versus preservation during the Paleocene–Eocene thermal maximum: evidence from Ba/Ca in foraminifera. International Conference on Paleoceanography VIII Program and Abstracts, Biarritz, France, p. 87.

Huber, M., 2002. Straw man 1: a preliminary view of the tropical Pacific from a global coupled climate model simulation of the early Paleogene. *In* Lyle, M., Wilson, P.A., Janecek, T.R., et al., *Proc. ODP, Init. Repts.,* 199, 1–30 [CD-ROM]. Available from: Ocean Drilling Program, Texas A&M University, College Station TX 77845-9547, USA.

Kelly, D.C., Bralower, T.J., Zachos, J.C., Premoli Silva, I., and Thomas, E., 1996. Rapid diversification of planktonic foraminifera in the tropical Pacific (ODP Site 865) during the Late Paleocene Thermal Maximum. *Geology,* 24:423–426.

Kennett, J.P., and Stott, L.D., 1991. Abrupt deep-sea warming, paleoceanographic changes and benthic extinctions at the end of the Palaeocene. *Nature (London U.K.),* 353:225–229.

Lyle, M., Wilson, P.A., Janecek, T.R., et al., 2002. *Proc. ODP, Init. Repts.,* 199 [CD-ROM]. Available from: Ocean Drilling Program, Texas A&M University, College Station TX 77845-9547, USA.

Miller, K.G., Fairbanks, R.G., and Mountain, G.S., 1987. Tertiary oxygen isotope synthesis, sea-level history, and continental margin erosion. *Paleoceanography,* 2:1–19.

Nilsen, E.B., Anderson, L.D., and Delaney, M.L., 2003. Paleoproductivity, nutrient burial, climate change and the carbon cycle in the western equatorial Atlantic across the Eocene/Oligocene boundary. *Paleoceanography,* 18(3):10.1029/2002PA000804.

Norris, R.D., and Röhl, U., 1999. Carbon cycling and chronology of climate warming during the Palaeocene/Eocene transition. *Nature (London U.K.),* 401:775–778.

Quintin, L.L., Faul, K.L., Lear, C., Graham, D., Peng, C., Murray, R.W., and Shipboard Scientific Party, 2002. Geochemical analysis of bulk marine sediment by inductively coupled plasma–atomic emission spectroscopy on board the *JOIDES Resolution*. *In* Lyle, M., Wilson, P.A., Janecek, T.R., et al., *Proc. ODP, Init. Repts.,* 199 [Online]. Available from World Wide Web: http://www-odp.tamu.edu/publications/199_IR/chap_07/chap_07.htm. [Cited YYYY-MM-DD]

Paytan, A., and Kastner, M., 1996. Benthic Ba fluxes in the central equatorial Pacific, implications for the oceanic Ba cycle. *Earth Planet. Sci. Lett.,* 142:439–450.

Paytan, A., Kastner, M., and Chavez, F., 1996. Glacial to interglacial fluctuations in productivity in the equatorial Pacific as indicated by marine barite. *Science,* 274:1355–1357.

Paytan, A., Kastner, M., Martin, E., Macdougall, J., and Herbert T., 1993. Marine barite as a monitor of seawater strontium isotope composition. *Nature (London U.K.),* 366:445–449.

Paytan, A., Mearon, S., Cobb, K., and Kastner, M., 2002. Origin of marine barite deposits: Sr and S isotope characterization. *Geology,* 30:747–750.

Ruttenberg, K.C., 1992. Development of a sequential extraction method for different forms of phosphorus in marine sediments. *Limnol. Oceanogr.,* 37:1460–1482.

Ruttenberg, K.C., and Berner, R.A., 1993. Authigenic apatite formation and burial in sediments from non-upwelling, continental margin environments. *Geochim. Cosmochim. Acta,* 57:991–1007.

Schmitz, B., Charisi, S.D., Thompson, E.I., and Speijer, R.P., 1997. Barium, SiO_2 (excess), and P_2O_5 as proxies of biological productivity in the Middle East during the Palaeocene and the latest Palaeocene benthic extinction event. *Terra Nova,* 9:95–99.

Stoll, H.M., and Bains, S., 2003. Coccolith Sr/Ca records of productivity during the Paleocene–Eocene Thermal Maximum from the Weddell Sea. *Paleoceanography,* 18(2):10.1029/2002PA000875.

Thomas, E., 1998. Biogeography of the late Paleocene benthic foraminiferal extinction. *In* Aubry, M.-P., Lucas, S.G., and Berggren, W.A., (Eds.), *Late Paleocene–Early Eocene Biotic and Climatic Events in the Marine and Terrestrial Records:* New York (Columbia Univ. Press), 214–243.

Thomas, E., and Shackleton, N., 1996. The Palaeocene–Eocene benthic foraminiferal extinction and stable isotope anomalies. *In* Knox, R.W.O'B., Corfield, R.M., and Dunay, R.E. (Eds.), *Correlation of the Early Paleogene in Northwest Europe.* Geol. Soc. Spec. Publ., 101:401–441.

Zachos, J.C., Lohmann, K.C., Walker, J.C.G., and Wise, S.W., Jr., 1993. Abrupt climate changes and transient climates during the Paleogene: a marine perspective. *J. Geol.,* 101:191–213.

Zachos, J.C., Wara, M.W., Bohaty, S., Delaney, M.L., Petrizzo, M.R., Brill, A., Bralower, T.J., and Premoli-Silva, I., 2003. A transient rise in tropical sea surface temperature during the Paleocene–Eocene Thermal Maximum. *Science,* 302:10.1126/science.1090110.

Figure F1. A. Total P from the four-step extraction process (Table T1, p. 20) and shipboard P (Table T3, p. 22) (Lyle, Wilson, Janecek, et al., 2002) vs. depth. **B.** Total P from the four-step extraction vs. shipboard P. Only the samples for which depth horizons exactly correspond are plotted. For linear regression, slope = 0.74 ± 0.06 and y-intercept = 0.07 ± 0.04; r^2 = 0.90. A 1:1 line is plotted for reference.

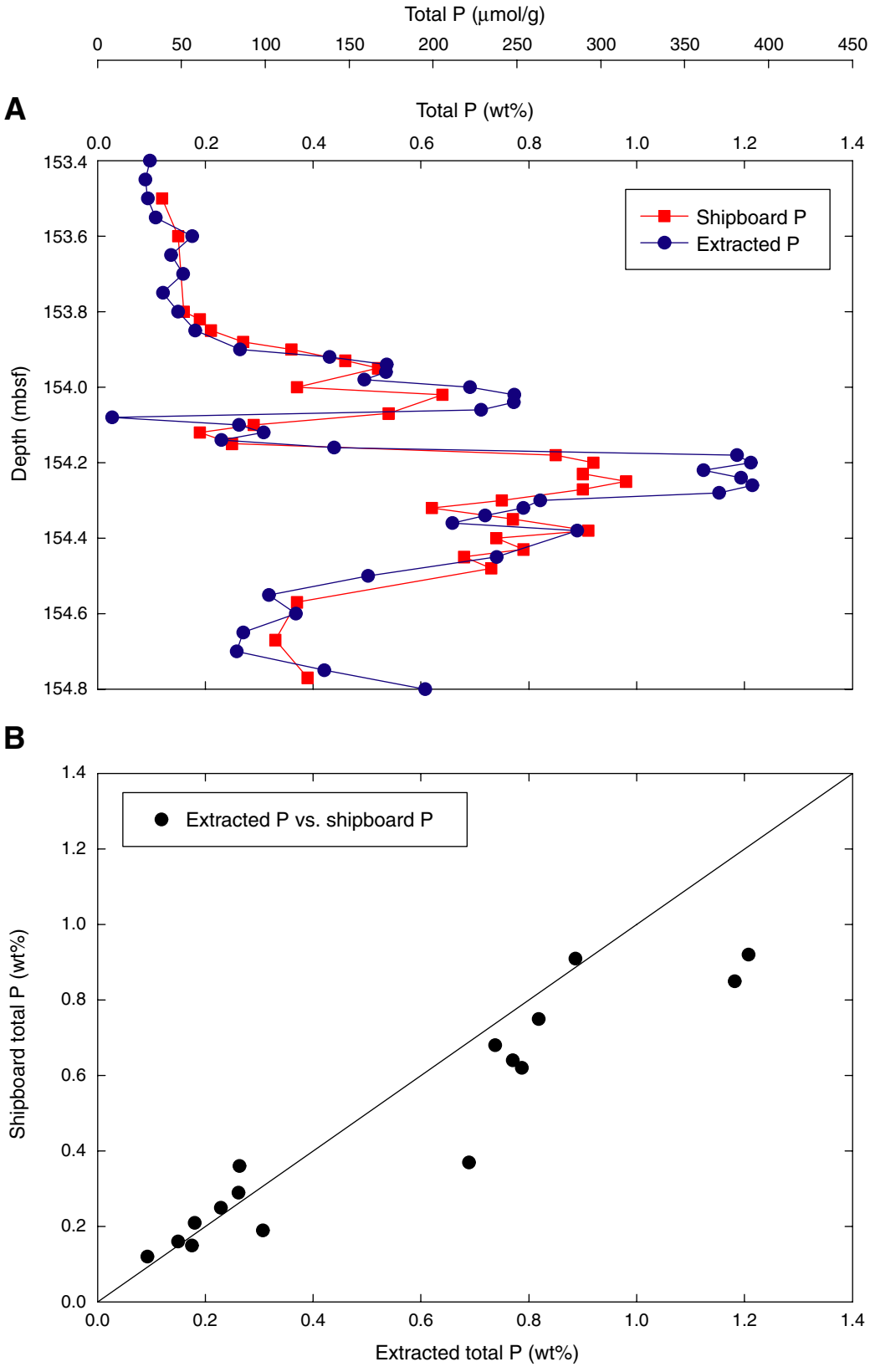

Figure F2. **A.** Barite (Table T1, p. 20) and shipboard Ba (Table T3, p. 22) (Lyle, Wilson, Janecek, et al., 2002) vs. depth. **B.** Barite vs. shipboard Ba. Only the samples to which depth horizons exactly correspond are plotted. For linear regression, slope = 0.75 ± 0.08 and y-intercept = 3300 ± 800; r^2 = 0.89.

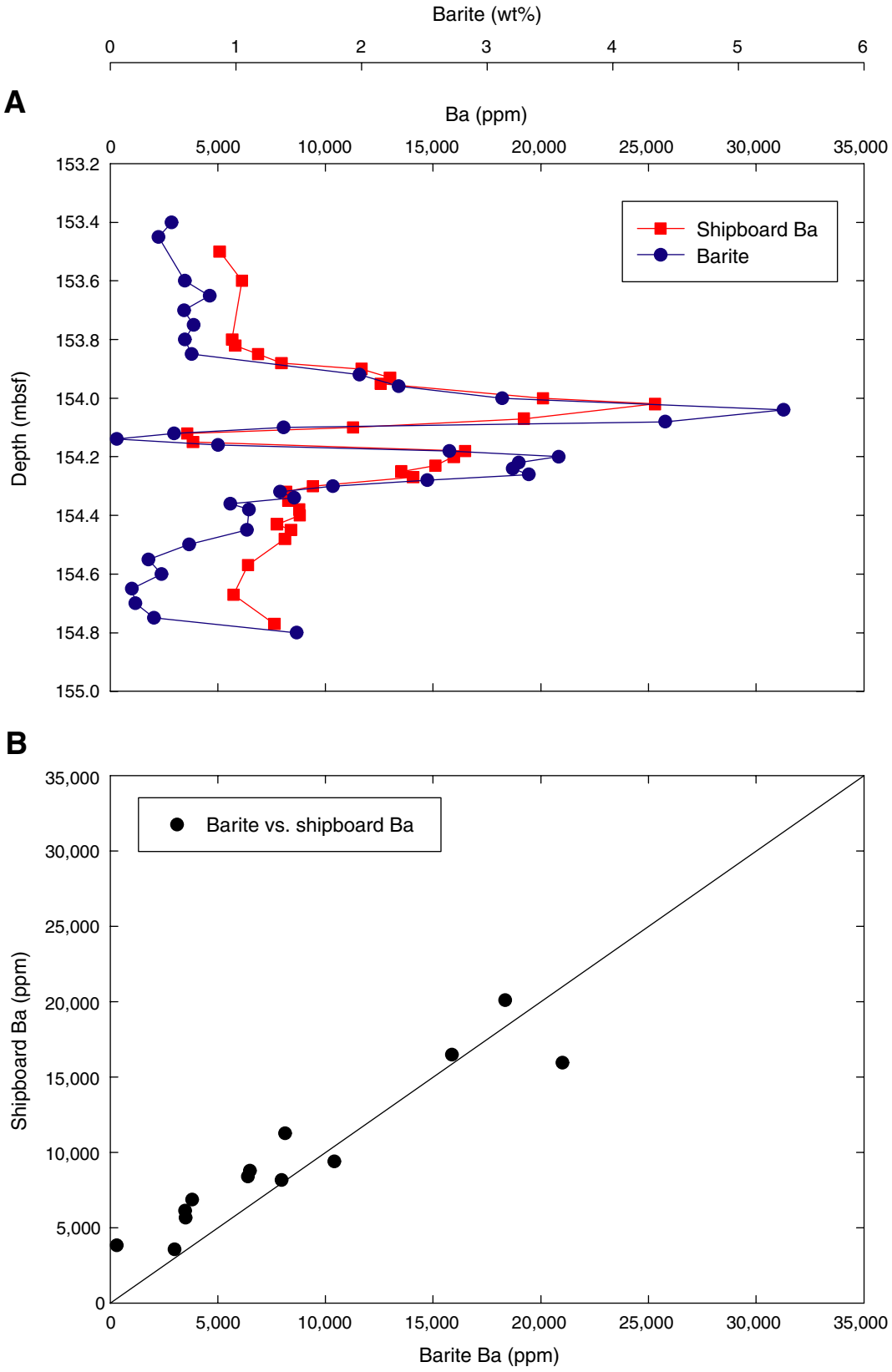

Figure F3. Geochemical components vs. depth for Section 199-1221C-11H-3. **A.** Reactive P (µmol P/g) and the sum of oxide-associated, organic, and authigenic P (and water-soluble P, when applicable). **B.** Detrital P (µmol P/g). **C.** Barite (wt%). **D.** $CaCO_3$ (wt%). **E.** Shipboard Mn (wt%) (Table T3, p. 22). See Table T1, p. 20, for reactive P, detrital P, and barite concentrations and "Methods," p. 4, and Table T2, p. 21, for typical analytical errors for these components. BEE = Benthic Extinction Event.

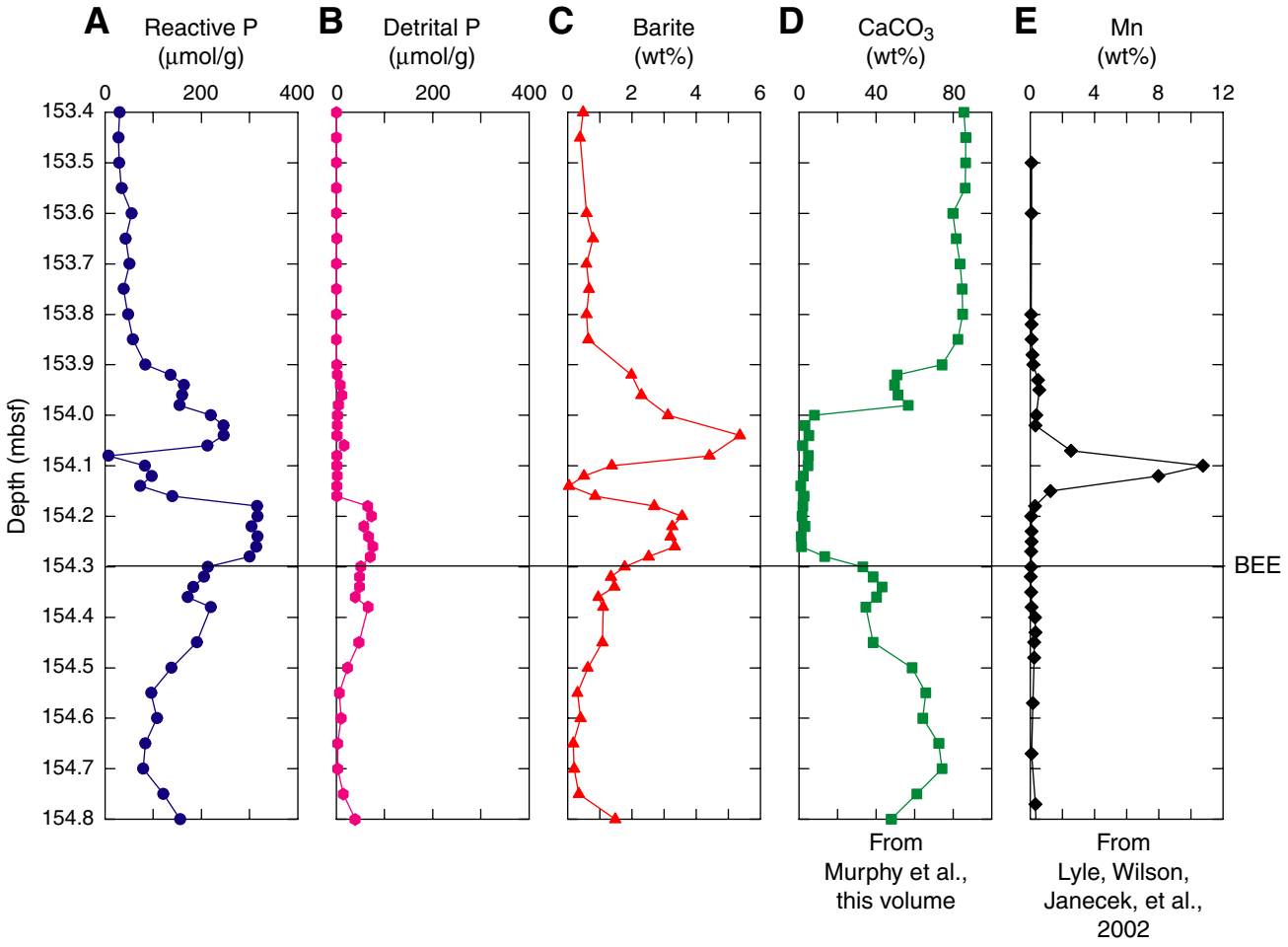

Figure F4. Geochemical components calculated on a $CaCO_3$-free basis and barite Ba to reactive P ratio vs. depth for Section 199-1221C-11H-3. **A.** $CaCO_3$-free reactive P (µmol P/g) and the sum of oxide-associated, organic, and authigenic P (and water-soluble P, when applicable). **B.** $CaCO_3$-free detrital P (µmol P/g). **C.** $CaCO_3$-free barite (wt%). **D.** $CaCO_3$-free organic carbon (wt%). **E.** Barite Ba to reactive P ratios. The ratio (1.4) for a modern equatorial Pacific core top (JGOFS TT013-69MC, 0.11°N, 139.72°W; 4307 mbsl) slightly west of the ODP Site 1221 Paleogene location is shown. To calculate barite Ba to reactive P values, some reactive P values from adjacent samples were averaged in order to compare them directly with the barite values (see Table T4, p. 23). $CaCO_3$-free data only calculated where data and $CaCO_3$ from Murphy et al. (this volume) have the same depth horizons. See Table T4, p. 23, for all concentrations. BEE = Benthic Extinction Event.

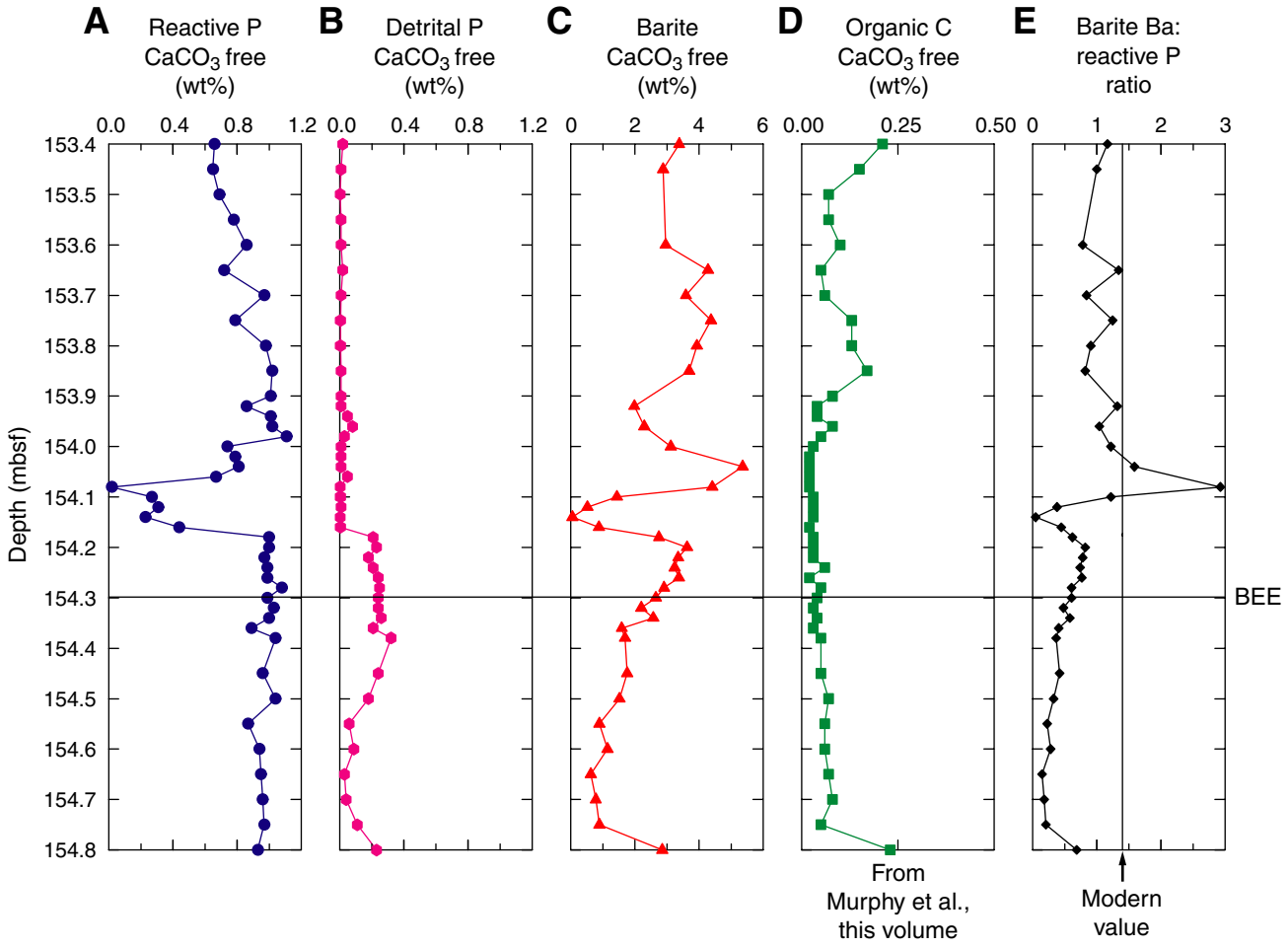

Table T1. Concentrations of phosphorus components and barite.

Core, section, interval (cm)	Depth (mbsf)	Phosphorus concentrations (µmol P/g sediment)														Barite (wt%)
		Water soluble		Oxide associated		Authigenic		Detrital		Organic		Reactive		Total		
		Mean	SD	Mean	SD	Mean	SD	Mean	SD	Mean	SD	Mean	SD	Mean	SD	
199-1221C-																
11X-3, 0–3	153.40	BDL	BDL	BDL	BDL	30.3	1.49	0.77	0.00	0.19	0.00	30.5	1.49	31.3	1.49	0.49
11X-3, 5–8	153.45	BDL	BDL	BDL	BDL	28.0	1.62	0.38	0.00	0.17	0.00	28.1	1.62	28.5	1.62	0.39
11X-3, 10–13	153.50	BDL	BDL	BDL	BDL	29.6	1.19	0.15	0.00	0.15	0.01	29.7	1.19	29.9	1.19	
11X-3, 15–18	153.55	0.76	0.04	0.35	0.18	33.2	0.66	0.23	0.00	0.18	0.01	34.5	0.68	34.7	0.68	
11X-3, 20–23	153.60	0.10	0.00	0.53	0.25	54.9	0.45	0.77	0.02	0.25	0.00	55.7	0.52	56.5	0.52	0.59
11X-3, 25–28	153.65	0.06	0.00	BDL	BDL	42.8	1.17	0.99	0.01	0.15	0.00	43.0	1.17	44.0	1.17	0.79
11X-3, 30–33	153.70	0.08	0.00	BDL	BDL	50.6	1.30	0.28	0.00	0.10	0.01	50.8	1.30	51.0	1.30	0.59
11X-3, 35–38	153.75	BDL	BDL	BDL	BDL	38.5	1.76	0.24	0.01	0.18	0.01	38.7	1.76	39.0	1.76	0.66
11X-3, 40–43	153.80	BDL	BDL	BDL	BDL	47.6	0.01	0.23	0.00	0.20	0.01	47.8	0.01	48.1	0.01	0.60
11X-3, 45–48	153.85	BDL	BDL	0.35	0.24	57.2	1.54	0.45	0.02	0.27	0.01	57.8	1.56	58.2	1.56	0.65
11X-3, 50–52	153.90	0.22	0.01	0.44	0.01	82.8	0.15	1.11	0.01	0.36	0.00	83.8	0.15	84.9	0.15	
11X-3, 50–54	153.92															1.98*
11X-3, 52–54	153.92	0.39	0.02	1.32	0.14	133.7	4.44	2.27	0.04	0.71	0.01	136.1	4.44	138.4	4.44	
11X-3, 54–56	153.94	0.52	0.02	0.51	0.18	162.0	3.69	8.52	0.40	0.81	0.00	163.8	3.70	172.4	3.72	
11X-3, 54–58	153.96															2.30*
11X-3, 56–58	153.96	0.89	0.04	0.68	0.27	157.5	3.75	11.97	0.58	0.94	0.03	160.0	3.76	171.9	3.81	
11X-3, 58–60	153.98	0.20	0.01	0.72	0.20	152.9	7.43	4.45	0.16	0.80	0.02	154.6	7.44	159.1	7.44	
11X-3, 58–62	154.00															3.12*
11X-3, 60–62	154.00	1.63	0.05	1.18	0.08	215.9	7.90	2.41	0.03	0.99	0.00	219.7	7.90	222.1	7.90	
11X-3, 62–64	154.02	2.39	0.12	1.69	0.23	240.8	5.45	2.32	0.01	1.12	0.03	246.0	5.46	248.3	5.46	
11X-3, 62–66	154.04															5.36*
11X-3, 64–66	154.04	2.44	0.11	2.97	0.05	239.8	5.77	1.74	0.00	1.17	0.04	246.1	5.77	248.2	5.77	
11X-3, 66–68	154.06	1.32	0.06	2.76	0.18	207.0	6.73	16.11	0.00	1.57	0.04	212.6	6.74	228.8	6.74	
11X-3, 66–70	154.08															4.42*
11X-3, 68–70	154.08	2.76	0.08	3.04	0.02	0.7	0.05	1.33	0.00	0.98	0.01	7.5	0.10	8.8	0.10	
11X-3, 70–72	154.10	0.13	0.01	1.43	0.04	80.5	0.05	1.50	0.00	0.82	0.02	82.9	0.07	84.4	0.07	1.38
11X-3, 72–74	154.12	0.14	0.01	1.20	0.04	95.3	3.88	1.92	0.06	0.46	0.00	97.0	3.88	99.0	3.88	0.51
11X-3, 74–76	154.14	0.54	0.04	0.81	0.23	71.3	0.08	0.88	0.00	0.40	0.01	73.1	0.24	74.0	0.24	0.05
11X-3, 76–78	154.16	0.72	0.02	1.24	0.03	136.9	4.13	1.42	0.07	0.76	0.02	139.6	4.13	141.0	4.13	0.86
11X-3, 78–80	154.18	0.19	0.01	5.20	0.37	307.9	11.50	65.50	2.76	2.42	0.01	315.7	11.46	381.2	11.8	2.70
11X-3, 80–82	154.20	0.16	0.02	4.86	0.07	309.0	9.95	72.93	0.03	2.57	0.03	316.5	9.95	389.5	9.95	3.57
11X-3, 82–84	154.22	0.61	0.03	4.12	0.02	297.3	1.75	56.93	0.86	2.36	0.04	304.4	1.75	361.3	1.95	3.25
11X-3, 84–86	154.24	0.43	0.03	4.42	0.08	308.9	7.57	67.06	0.03	2.79	0.14	316.6	7.57	383.6	7.57	3.20
11X-3, 86–88	154.26	0.48	0.03	4.84	0.03	306.4	11.00	76.22	3.65	2.39	0.02	314.1	11.00	390.4	11.5	3.33
11X-3, 88–90	154.28	0.11	0.00	6.31	0.07	291.6	6.91	70.30	2.18	2.22	0.01	300.2	6.91	370.5	7.24	2.53
11X-3, 90–92	154.30	1.22	0.11	2.09	0.04	208.6	9.81	50.70	0.04	1.28	0.02	213.2	9.81	263.9	9.81	1.77
11X-3, 92–94	154.32	0.22	0.01	1.38	0.04	201.5	6.24	48.39	0.16	2.33	0.05	205.4	6.24	253.8	6.24	1.35
11X-3, 94–96	154.34			2.77	0.06	177.1	0.00	48.07	0.61	3.07	0.01	182.9	0.06	231.0	0.61	1.46
11X-3, 96–98	154.36			2.26	0.30	167.0	0.57	39.67	0.32	2.60	0.01	171.9	0.65	211.5	0.72	0.96
11X-3, 98–100	154.38			3.24	0.21	211.9	0.29	66.31	0.03	4.48	0.02	219.6	0.36	285.9	0.36	1.10
11X-3, 105–108	154.45			2.66	0.01	184.9	0.28	47.10	0.13	3.21	0.01	190.8	0.28	237.9	0.31	1.09
11X-3, 110–113	154.50			2.12	0.03	133.9	0.00	23.34	0.02	1.95	0.01	138.0	0.03	161.3	0.04	0.63
11X-3, 115–118	154.55			1.29	0.02	93.8	0.56	6.17	0.03	0.91	0.00	96.0	0.56	102.2	0.57	0.31
11X-3, 120–123	154.60			1.61	0.03	105.6	0.84	10.08	0.03	0.99	0.04	108.1	0.84	118.2	0.85	0.41
11X-3, 125–128	154.65			3.05	2.74	80.2	0.57	2.92	0.01	0.76	0.02	84.0	2.80	86.9	2.80	0.17
11X-3, 130–133	154.70			1.06	0.04	76.5	0.57	3.32	0.01	2.18	0.00	79.7	0.57	83.0	0.57	0.20
11X-3, 135–138	154.75			2.01	0.05	117.3	0.28	14.32	0.19	1.61	0.00	120.9	0.28	135.2	0.34	0.35
11X-3, 140–142	154.80			2.73	0.02	150.5	0.28	39.02	0.33	3.02	0.01	156.2	0.29	195.3	0.44	1.49

Notes: SD = standard deviation. BDL = below detection limit. Blank fields = the parameter was not measured for the given sample. * = Combined samples for barite separations.

Table T2. Analytical figures of merit.

	Phosphorus Concentration (µmol P/g sediment)						
	Water soluble	Oxide associated	Authigenic	Organic	Detrital	Reactive	Total
Detection Limits*	0.03	0.3	0.41	0.05	0.06	NA	NA
Reproducibility of consistency standards†							
North Atlantic‡	NA	0.83 ± 0.66	9.39 ± 0.87	0.60 ± 0.17	0.38 ± 0.20	10.30 ± 1.02	10.66 ± 1.07
Southern Ocean**	NA	0.47 ± 0.16	11.12 ± 0.65	0.40 ± 0.14	1.08 ± 0.41	11.60 ± 0.59	12.67 ± 0.51

Notes: * = defined as three times the standard deviation of replicate measures of a low-concentration solution standard and expressed in equivalent concentration for a sediment sample. † = long-term analytical reproducibility was assessed by calculation of the mean P concentrations ±1σ for two sedimentary consistency standards. ‡ = the North Atlantic consistency standard was composed of a mixture of samples from ODP Sites 1050–1052. ** = the Southern Ocean consistency standard was composed of a mixture of samples from ODP Sites 689, 690, and 738. NA = not applicable.

Table T3. Shipboard P, Ba, and Mn.

Core, section, interval (cm)	Depth (mbsf)	Total		
		P (wt%)	Ba (ppm)	Mn (wt%)
199-1221C-				
11X-3, 10–12.5	153.50	0.12	5,089	0.08
11X-3, 20–22.5	153.60	0.15	6,123	0.09
11X-3, 40–42.5	153.80	0.16	5,665	0.07
11X-3, 42.5–45	153.82	0.19	5,807	0.08
11X-3, 45–47.5	153.85	0.21	6,869	0.10
11X-3, 47.5–50	153.88	0.27	7,956	0.13
11X-3, 50–52.5	153.90	0.36	11,673	0.20
11X-3, 52.5–55	153.93	0.46	12,996	0.48
11X-3, 55–57.5	153.95	0.52	12,568	0.56
11X-3, 60–62.5	154.00	0.37	20,098	0.38
11X-3, 62.5–67.5	154.02	0.64	25,308	0.32
11X-3, 67.5–70	154.07	0.54	19,220	2.53
11X-3, 70–72.5	154.10	0.29	11,276	10.76
11X-3, 72.5–75	154.12	0.19	3,570	7.98
11X-3, 75–77.5	154.15	0.25	3,847	1.26
11X-3, 77.5–80	154.18	0.85	16,482	0.30
11X-3, 80–82.5	154.20	0.92	15,956	0.07
11X-3, 82.5–85	154.23	0.90	15,108	0.08
11X-3, 85–87.5	154.25	0.98	13,514	0.10
11X-3, 87.5–90	154.27	0.90	14,065	0.05
11X-3, 90–92.5	154.30	0.75	9,415	0.05
11X-3, 92.5–95	154.32	0.62	8,175	0.04
11X-3, 95–97.5	154.35	0.77	8,280	0.05
11X-3, 97.5–100	154.38	0.91	8,785	0.08
11X-3, 100–102.5	154.40	0.74	8,805	0.29
11X-3, 102.5–105	154.43	0.79	7,744	0.33
11X-3, 105–107.5	154.45	0.68	8,395	0.25
11X-3, 107.5–110	154.48	0.73	8,117	0.26
11X-3, 117–119.5	154.57	0.37	6,407	0.18
11X-3, 127–129.5	154.67	0.33	5,720	0.09
11X-3, 137–139.5	154.77	0.39	7,624	0.32

Note: Data from Lyle, Wilson, Janecek, et al., 2002.

Table T4. $CaCO_3$ and $CaCO_3$-free reactive P, detrital P, barite, organic carbon, Mn, and reactive P ratios.

Core, section, interval (cm)	Depth (mbsf)	$CaCO_3$ (wt%)*	$CaCO_3$ free (wt%)						
			Reactive P	Detrital P	Barite	Organic carbon*	Mn†	Organic C to reactive P ratio	Barite Ba to reactive P ratio
199-1221C-									
11X-3, 0–3	153.40	85.59	0.66	0.017	3.39	0.21		0.82	1.17
11X-3, 5–8	153.45	86.60	0.65	0.009	2.88	0.15		0.59	1.00
11X-3, 10–13	153.50	86.55	0.69	0.003		0.07	0.59	0.28	
11X-3, 15–18	153.55	86.23	0.78	0.005		0.07		0.24	
11X-3, 20–23	153.60	79.94	0.86	0.012	2.96	0.10	0.45	0.30	0.78
11X-3, 25–28	153.65	81.55	0.72	0.017	4.29	0.05		0.19	1.34
11X-3, 30–33	153.70	83.70	0.97	0.005	3.60	0.06		0.16	0.84
11X-3, 35–38	153.75	84.83	0.79	0.005	4.38	0.13		0.43	1.25
11X-3, 40–43	153.80	84.89	0.98	0.005	3.94	0.13	0.46	0.35	0.91
11X-3, 45–48	153.85	82.47	1.02	0.008	3.70	0.17	0.57	0.43	0.82
11X-3, 50–52	153.90	74.37	1.01	0.013		0.08	0.78	0.20	
11X-3, 50–54	153.92	62.69‡	0.91‡		5.32**				1.32
11X-3, 52–54	153.92	51.00	0.86	0.014		0.04		0.12	
11X-3, 54–56	153.94	49.67	1.01	0.052		0.04		0.10	
11X-3, 54–58	153.96	50.51‡	1.01‡		4.64**				1.04
11X-3, 56–58	153.96	51.35	1.02	0.076		0.08		0.21	
11X-3, 58–60	153.98	56.67	1.11	0.032		0.05		0.11	
11X-3, 58–62	154.00	32.42‡	0.86‡		4.62**				1.22
11X-3, 60–62	154.00	8.17	0.74	0.008		0.03	0.41	0.11	
11X-3, 62–64	154.02	3.12	0.79	0.007		0.02	0.33	0.07	
11X-3, 62–66	154.04	4.17‡	0.80‡		5.60**				1.59
11X-3, 64–66	154.04	5.22	0.81	0.006		0.02		0.07	
11X-3, 66–68	154.06	1.94	0.67	0.051		0.02		0.08	
11X-3, 66–70	154.08	3.42‡	0.35‡		4.58**				2.93
11X-3, 68–70	154.08	4.89	0.02	0.004		0.02		2.22	
11X-3, 70–72	154.10	4.80	0.27	0.005	1.45	0.03	11.30	0.30	1.22
11X-3, 72–74	154.12	2.37	0.31	0.006	0.52	0.03	8.17	0.26	0.38
11X-3, 74–76	154.14	1.06	0.23	0.003	0.05	0.03		0.34	0.05
11X-3, 76–78	154.16	2.64	0.44	0.005	0.88	0.02		0.12	0.45
11X-3, 78–80	154.18	2.09	1.00	0.207	2.76	0.03	0.31	0.08	0.62
11X-3, 80–82	154.20	1.66	1.00	0.230	3.63	0.03	0.07	0.08	0.82
11X-3, 82–84	154.22	3.11	0.97	0.182	3.36	0.03		0.08	0.78
11X-3, 84–86	154.24	1.14	0.99	0.210	3.24	0.06		0.16	0.74
11X-3, 86–88	154.26	1.37	0.99	0.240	3.38	0.02		0.05	0.77
11X-3, 88–90	154.28	13.49	1.08	0.252	2.92	0.05		0.11	0.61
11X-3, 90–92	154.30	33.25	0.99	0.235	2.66	0.04	0.07	0.12	0.61
11X-3, 92–94	154.32	38.47	1.03	0.244	2.20	0.03	0.07	0.08	0.48
11X-3, 94–96	154.34	43.14	1.00	0.262	2.57	0.04		0.09	0.58
11X-3, 96–98	154.36	40.24	0.89	0.206	1.60	0.03		0.10	0.41
11X-3, 98–100	154.38	34.81	1.04	0.315	1.69	0.05	0.12	0.11	0.37
11X-3, 105–108	154.45	38.57	0.96	0.238	1.77	0.05	0.41	0.13	0.42
11X-3, 110–113	154.50	58.85	1.04	0.176	1.52	0.07		0.18	0.33
11X-3, 115–118	154.55	65.83	0.87	0.056	0.89	0.06		0.17	0.23
11X-3, 120–123	154.60	64.33	0.94	0.088	1.15	0.06		0.15	0.28
11X-3, 125–128	154.65	72.65	0.95	0.033	0.63	0.07		0.20	0.15
11X-3, 130–133	154.70	74.38	0.96	0.040	0.79	0.08		0.21	0.18
11X-3, 135–138	154.75	61.23	0.97	0.115	0.90	0.05		0.14	0.21
11X-3, 140–142	154.80	47.96	0.93	0.232	2.85	0.23		0.64	0.69

Notes: * = Data from **Murphy et al.,** this volume. † = Mn $CaCO_3$-free data only calculated where shipboard Mn and $CaCO_3$ from Murphy et al. (this volume) have same depth horizons. ‡ = Average of values for the two 2-cm intervals that comprise this depth interval, calculated for $CaCO_3$ and reactive P, to compare these values to the barite values for the combined samples. ** = Combined samples for barite separations.